Title:

Temporal profile of betatron radiation from laser-driven electron accelerators

Authors:

Vojtěch Horný, Jaroslav Nejdl, Michaela Kozlová, Miroslav Krůs, Karel Boháček, Václav Petržílka, and Ondřej Klimo

Final manuscript

The original publication may be found at:

Journal: Physics of Plasmas 24, 063107 (2017)

DOI: http://dx.doi.org/10.1063/1.4985687

Temporal Profile of Betatron Radiation from Laser-Driven Electron Accelerators

Vojtěch Horný,[1,2,3,a)] Jaroslav Nejdl,[1,2] Michaela Kozlová,[1,2] Miroslav Krůs,[1,2] Karel Boháček,[2,3] Václav Petržílka,[1] and Ondřej Klimo[2,3]

[1)] *Institute of Plasma Physics, Czech Academy of Sciences, Za Slovankou 1782/3, 182 00 Praha 8, Czech Republic*

[2)] *Institute of Physics, Czech Academy of Sciences, Na Slovance 1999/2, 182 21, Praha 8, Czech Republic*

[3)] *Faculty of Nuclear Sciences and Physical Engineering, Czech Technical University in Prague, Břehová 7, 115 19 Praha 1, Czech Republic*

(Dated: 15 May 2017)

Temporal profile of X-ray betatron radiation was theoretically studied for the parameters available with current laser systems. Characteristics of the betatron radiation were investigated for three different configurations of laser wakefield acceleration: typical self-injection regime and optical injection regime with perpendicularly crossed injection and drive beams, both achievable with 100 TW class laser, and ionization injection regime with sub-10 TW laser system that was experimentally verified. Constructed spectrograms demonstrate that X-ray pulse durations are in order of few tens of femtoseconds and the optical injection case reveals the possibility of generating X-ray pulses as short as 2.6 fs. X-ray pulse duration depends mainly on the length of the trapped electron bunch as the emitted photons copropagate with the bunch with nearly the same velocity. These spectrograms were calculated using novel simplified method based on the theory of Liénard-Wiechert potentials. It takes advantage of the fact that the electron oscillates transversally in the accelerating plasma wave in the wiggler regime and, thus, emits radiation almost exclusively in the turning points of its sine-like trajectory. Therefore there are only few very narrow time intervals, which contribute significantly to the emission of radiation, while the rest can be neglected. These narrow time intervals are determined from the electron trajectories calculated using particle-in-cell simulations and the power spectrum at given point in far field is computed for each electron using the Fourier transform. Spectrograms of the emitted radiation are constructed by summing contributions of individual particles, since the incoherent nature of the electron bunch is assumed.

Keywords: betatron radiation, laser wakefield acceleration, X-rays, wiggler regime, spectrogram

I. INTRODUCTION

Interaction of ultrashort laser pulses with relativistic intensities with gas targets has recently led to the development of novel X-ray sources[1]. One of these sources is based on the betatron oscillations[2,3] of relativistic electrons in the beam, which is being accelerated by the laser wakefield acceleration (LWFA) mechanism[4,5]. Such compact sources provide intense incoherent femtosecond X-ray pulses with low divergence beams, which may find application in fundamental science, industry or medicine[6–10].

Typical vibrational period in the atoms is in the order of tens of femtoseconds[11]. Once having an X-ray source producing even shorter pulses, the fundamental physical processes such as electron transfer, lattice vibrations, phase transitions, chemical reactions or a spin dynamics could be sampled and therefore possibly better understood. The information about duration and even temporal profile of the laser produced betatron X-ray pulse is therefore very important.

This paper proposes a method to numerically estimate properties of X-rays emitted by an electron bunch accelerated using the mechanism of LWFA, if the electron trajectories are known, e.g. from the numerical particle-in-cell (PIC) simulation. Furthermore, as trapped electrons perform betatron oscillations in the wiggler regime, the temporal profile of the emitted radiation (spectrogram) can be constructed by simply summing the spectral power contributions of individual electrons. The method in its present form is not intended to be used when very high energy X-rays ($E_{ph} > 10$ MeV) are generated, since quantum effects are neglected here.

The calculations performed using this method confirm that the generated X-ray pulse duration is typically shorter than laser pulse duration, and pulses even shorter than 3 fs could be generated. The calculations also open the way for optimizing the X-ray pulse duration and even pulse shape through different electron injection mechanisms. Such pulses could be convenient for sampling of ultrafast fundamental physical processes.

This paper is organized as follows. In section II the general method to calculate the betatron radiation properties from the electron trajectory is introduced. It is simplified for the wiggler regime of betatron oscillations, and the method to construct the radiation spectrograms is derived. The section III uses the method for calculation of radiation characteristics for three different configura-

[a)] Electronic mail: horny@pals.cas.cz

tions of laser wakefield acceleration. The conclusions are summarized in section IV.

II. CALCULATION OF RADIATION EMITTED BY MOVING CHARGE

A. General method

Presented method is complementary to the previous treatments proposed by Thomas[12] and by Chen[13], which are based on the solution of the integral

$$\frac{\mathrm{d}^2 I}{\mathrm{d}\omega \mathrm{d}\Omega} = \frac{e^2}{16\pi^3 \varepsilon_0 c} \times \left| \int_{-\infty}^{\infty} \mathrm{e}^{i\omega\left(t' - \frac{\mathbf{n}\cdot\mathbf{r}(t')}{c}\right)} \times \frac{\mathbf{n}\times[(\mathbf{n}-\boldsymbol{\beta})\times\dot{\boldsymbol{\beta}}]}{(1-\boldsymbol{\beta}\cdot\mathbf{n})^2} \mathrm{d}t' \right|^2 . \quad (1)$$

representing the spectral intensity of radiation at a distance far compared with the scale of the emission region. The quantity ω is photon frequency, $\mathrm{d}\Omega$ is a solid angle centred on the direction of observation $\mathbf{n}$, e is electron charge, ε_0 is vacuum permittivity, c is speed of light in vacuum, $\mathbf{r}$ is electron position, $\boldsymbol{\beta}$ is a normalised velocity of electron, $\dot{\boldsymbol{\beta}} = \frac{\mathrm{d}\boldsymbol{\beta}}{\mathrm{d}t'}$ and t' is retarded time, which is connected with the observer's time t by the relation

$$t' = t - \frac{|\mathbf{R}|}{c}, \quad (2)$$

where $|\mathbf{R}| = R$ is a distance between electron and observer. Schematic illustration of the introduced quantities is depicted in Figure 1.

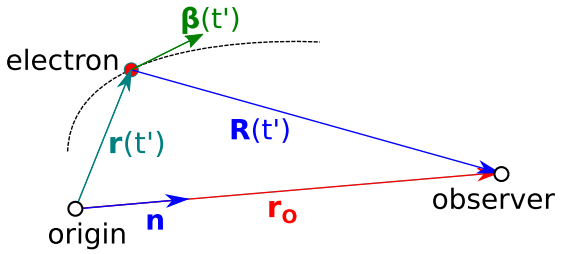

FIG. 1. Schematic illustration of discussed quantities.

Whereas Thomas's approach is based on semi-analytical integration of (1) and Chen integrates (1) by parts, the method presented here does not employ the radiation integral (1), but it is based on Fourier transform of the temporal profile of the electric field received by an observer. Electric field can be determined from the knowledge of the electron trajectory using the theory of electrodynamics, namely Liénard-Wiechert potentials.

The electric field at the position of the observer $\mathbf{r_O} = \mathbf{R} + \mathbf{r} \approx \mathbf{R}$ emitted by relativistic electron is[14]

$$\mathbf{E}(\mathbf{r_O}, t) = \frac{e}{4\pi\varepsilon_0} \times \left\{ \frac{(1-\boldsymbol{\beta}^2)(\mathbf{n}-\boldsymbol{\beta})}{R^2(1-\mathbf{n}\cdot\boldsymbol{\beta})^3} + \frac{\mathbf{n}\times[(\mathbf{n}-\boldsymbol{\beta})\times\dot{\boldsymbol{\beta}}]}{cR(1-\boldsymbol{\beta}\cdot\mathbf{n})^3} \right\}_{ret} . \quad (3)$$

The electric field (3) comprises of two terms, the first one called velocity field is decreasing as an inverse square of distance and the second one called acceleration field is inversely proportional to distance. The subscript *ret* means that the quantities are evaluated in retarded time. Similarly as in derivation of (1)[14] it is possible to neglect the first term of (3) and to consider only the acceleration field assuming an observer far away from the emission region. The dependence on the position $\mathbf{r_O}$ is omitted further in the text for the same reason.

The total energy radiated per unit solid angle by relativistic electron is[14]

$$\frac{\mathrm{d}\mathcal{E}}{\mathrm{d}\Omega} = c\varepsilon_0 \int_{-\infty}^{+\infty} |R(t)\mathbf{E}(t)|^2 \mathrm{d}t. \quad (4)$$

Applying Parseval's theorem from the Fourier analysis, the equation (4) can be reformulated as

$$\frac{\mathrm{d}\mathcal{E}}{\mathrm{d}\Omega} = \frac{c\varepsilon_0}{2\pi} \int_{-\infty}^{+\infty} |\mathfrak{F}[R(t)\mathbf{E}(t)](\omega)|^2 \mathrm{d}\omega = \frac{c\varepsilon_0}{\pi} \int_{0}^{+\infty} |\mathfrak{F}[R(t)\mathbf{E}(t)](\omega)|^2 \mathrm{d}\omega, \quad (5)$$

where $\mathfrak{F}$ is the symbol of Fourier transform. Hence, the spectral intensity of radiation emitted by a single electron can be written as

$$\frac{\mathrm{d}^2 I}{\mathrm{d}\omega \mathrm{d}\Omega} = \frac{c\varepsilon_0}{\pi} |\mathfrak{F}[R(t)\mathbf{E}(t)](\omega)|^2 . \quad (6)$$

The core of the method is to perform the Fourier transform of the quantity $\mathbf{E}(t)R(t)$. This quantity must be properly sampled in order to be able to calculate the spectrum of emitted X-rays. The minimum sampling frequency is determined by Nyquist-Shannon sampling theorem[15]. It states that the accurate reconstruction of the continuous signal whose frequencies are limited is possible only if the sampling frequency is higher than twice the highest frequency component of the sampled signal.

In practice, if the radiation energy spectrum is calculated up to the energy 15 keV, the corresponding photon frequency is 3.64×10^{18} Hz, sampling frequency of the signal should be 7.28×10^{18} Hz and it means that the length of the time step Δt of the electric field in the observer's frame of reference must be shorter than 0.137 as. If the radiation bandwidth reaches as far as 1 MeV, such a time step has to be at most 2.06 zs long. In comparison, a typical time step in PIC simulations of LWFA is 0.01–0.1 fs[16].

Furthermore, sampling in the observer's time t is usually not equidistant. The interpolation of the function $\mathbf{E}(t)R(t)$ must be carried out to obtain better sampling. Various interpolation methods may be used; however shape-preserving piecewise cubic interpolation offers satisfactory results with respect to the computational time demands. Once the interpolated signal $\mathbf{E}(t)R(t)$ is sampled properly, its fast Fourier transform can be computed.

A certain alternative for the low energy radiation can be non-uniform fast Fourier transform algorithm (NUFFT)[17]. However, it was not used for our calculations.

B. Betatron oscillations

In laser plasma accelerators, the trapped electron is accelerated longitudinally and wiggled transversally by wakefields formed behind the driver laser pulse. The transverse motion is sine-like[1] with the varying betatron frequency $\omega_\beta = \omega_p/(2\gamma)$, where $\gamma = 1/\sqrt{1-\boldsymbol{\beta}^2}$ is Lorentz factor and $\omega_p = (n_e e^2/m_e\varepsilon_0)^{1/2}$ is plasma frequency. Properties of the emitted radiation depend on strength parameter

$$K = r_\beta k_p \sqrt{\frac{\gamma}{2}}, \tag{7}$$

where r_β is betatron transverse amplitude of motion and $k_p = \omega_p/c$, on the betatron frequency ω_β, and on the electron energy $E_e = \gamma m_e c^2$.

The undulator regime is characterized by $K \ll 1$, the on axis spectrum is almost monochromatic with the fundamental frequency $\omega = 2\gamma^2\omega_\beta/(1+K^2/2)$. The wiggler regime occurs when $K \gg 1$, the spectrum is comprised of many very closely spaced harmonics of the fundamental frequency and can be characterized by the critical frequency

$$\omega_c = \frac{3}{2} K \gamma^2 \omega_\beta \tag{8}$$

that represents the median in the emitted power spectrum.

Without loss of generality, let us assume that the electron propagates in the x-direction and performs transverse betatron oscillations in the y-direction. Then $|E_x/E_y| \ll 1$ and $|E_z/E_y| \ll 1$, and therefore

$$|\mathfrak{F}[R(t)\mathbf{E}(t)](\omega)| \approx |\mathfrak{F}[R(t)E_y(t)](\omega)|\,.$$

Hence, it is possible to neglect the contributions of the electric field components E_x and E_z. The quantity $E_y(t)R(t)$ for two different electron trajectories is plotted in Figures 2a and 2c. Additionally, corresponding far field spectra on the axis of electron propagation are shown in Figures 2b and 2d. Electron trajectories were calculated using the simple model

$$y(t) = r_\beta \sin(\omega_\beta t), \tag{9}$$

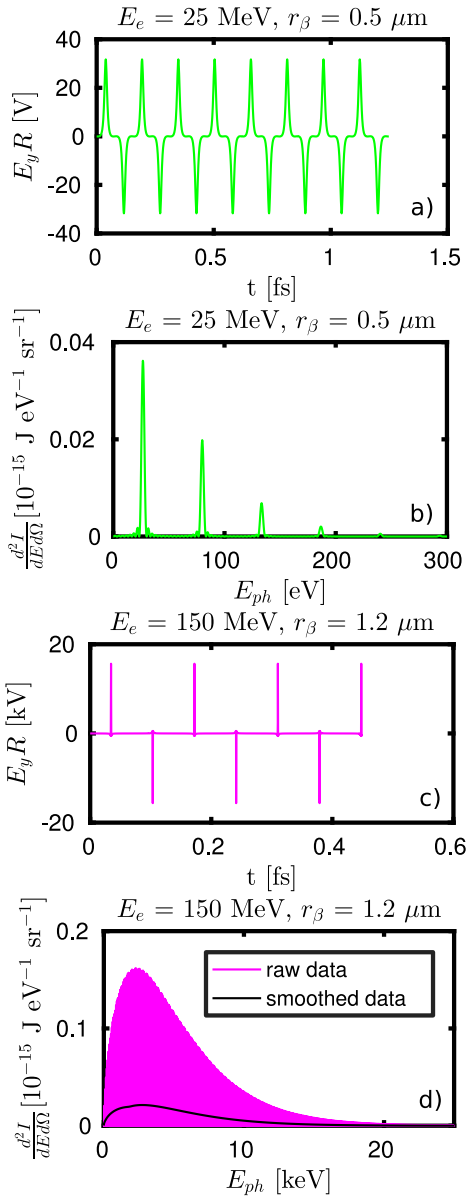

FIG. 2. Electric field and radiated spectrum by a moving electron on axis in two cases of electron energies and amplitudes of the betatron oscillations. a), b) transition state between undulator and wiggler with $E_e = 25$ MeV, $r_\beta = 0.5$ µm, $K = 1.0$. c), d) wiggler case with $E_e = 150$ MeV, $r_\beta = 1.2$ µm, $K = 5.5$. Black line represents spectrum smoothed using moving average window technique.

for the ambient electron density $n_e = 5 \times 10^{18}$ cm^{-3}. Electron propagated for 4 ps. The time durations t in Figures 2a and 2c corresponds to the inertial reference frame of the observer.

A transition state between undulator and wiggler regime ($K = 1$) is shown in Figures 2a and 2b. Fourier series comprise only of several odd harmonics. Figures 2c and 2d represent example of wiggler regime (for $K = 5.5$). The black line in the Figure 2d represents spectrum smoothed using moving average window tech-

nique. [1] Critical energy of radiation, calculated as median in the spectral intensity on axis divided by the factor of 1.54 [2], is 2.70 keV in this case, which is in the agreement with the expectation according to the formula[1]

$$h\omega_c \text{ [eV]} = 5.24 \times 10^{-21} \gamma^2 n_e[\text{cm}^{-3}] r_\beta[\mu\text{m}]. \quad (10)$$

The experimental data have shown that the betatron radiation occurs dominantly in the wiggler regime[21–24] and it was demonstrated that the spectrum of betatron radiation in the wiggler regime is synchrotron-like[25].

C. Simplification of the method for the wiggler case

It can be understood from Figure 2c that in the wiggler case, the electron emits radiation almost exclusively in the turning points of its sine-like trajectory. Hence, there are only few very narrow time intervals, which contribute significantly to the betatron radiation emission, while the rest can be neglected.

Analogical behaviour was observed also previously for different phenomenon[26]. It was shown that the trajectory of an electron oscillating in the field of relativistic laser pulse is comprised of relatively long rectilinear segments with the short looping turn between them. The temporal evolution of the electric field $\mathbf{E}(t)R(t)$ is therefore similar as the one in Figure 2c.

Let us consider the signal of the radiation $\mathbf{u}(t) = \mathbf{E}(t)R(t)$ as a sum of the contributions by single peaks $\mathbf{u}_j(t)$, i.e.

$$\mathbf{u}(t) = \sum_{j=1}^{N_p} \mathbf{u}_j(t), \quad (11)$$

where N_p is number of peaks. Each contribution can be written as

$$\mathbf{u}_j(t) = \begin{cases} \mathbf{E}(t)R(t) & |t - t_j| < \Delta t \\ 0 & \text{otherwise,} \end{cases} \quad (12)$$

where t_j are the times of the signal peaks and Δt is a width of the considered peaks. This width has to include whole peak and cannot overlap to its neighbours.

[1] Moving average window technique is a standard statistical tool to analyze data points by creating series of averages of partial subsets of the full data set in order to smooth out short-term fluctuations and highlight longer-term trends or cycles[18]. The size of inner subsets was 1/25000 of the full radiation spectrum bandwidth in examples presented in this paper.

[2] Median in the the synchrotron radiation spectral intensity on axis $\left.\frac{\mathrm{d}^2 I}{\mathrm{d}E\mathrm{d}\Omega}\right|_{\theta=0}$ is 1.54× higher than median in the angularly integrated spectral intensity $\frac{\mathrm{d}I}{\mathrm{d}E}$ [19], which is one of the characteristics of the critical energy[14]. See also an explanation in[20], but avoid the confusion due to different definitions of the critical energy.

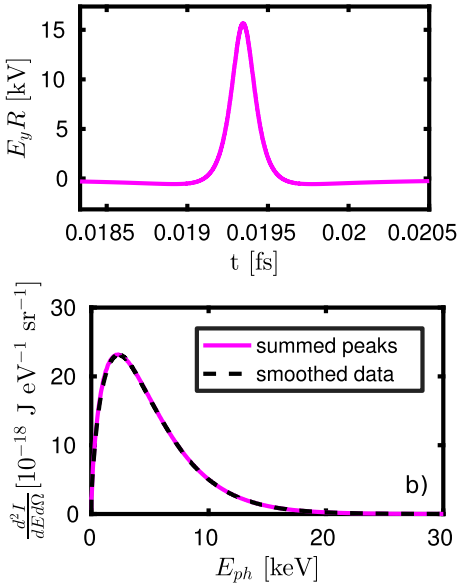

FIG. 3. a) One peak of the radiation signal $E_y(t)R(t)$ from the wiggler case in the Figure 2c). b) Corresponding spectrum calculated as a sum of the contributions by single peaks (magenta solid) and a smoothed spectrum calculated according to the equation (6) using the Fourier transform of the whole signal (black dashed).

The equation for the radiated energy per solid angle (4) can be in this case reformulated to

$$\frac{\mathrm{d}\mathcal{E}}{\mathrm{d}\Omega} = c\varepsilon_0 \int_{-\infty}^{+\infty} \left| \sum_{j=1}^{N_p} \mathbf{u}_j(t) \right|^2 \mathrm{d}t. \quad (13)$$

Thanks to the fact that the contributions of the single peaks do not overlap, the square of the absolute value of the sum of the contributions is equal to the sum of the squares of the single contributions

$$\frac{\mathrm{d}\mathcal{E}}{\mathrm{d}\Omega} = c\varepsilon_0 \int_{-\infty}^{+\infty} \sum_{j=1}^{N_p} |\mathbf{u}_j(t)|^2 \, \mathrm{d}t \quad (14)$$

and thanks to the sum rule

$$\frac{\mathrm{d}\mathcal{E}}{\mathrm{d}\Omega} = c\varepsilon_0 \sum_{j=1}^{N_p} \int_{-\infty}^{+\infty} |\mathbf{u}_j(t)|^2 \, \mathrm{d}t. \quad (15)$$

Using once again Parseval's theorem and sum rule we obtain

$$\begin{aligned} \frac{\mathrm{d}\mathcal{E}}{\mathrm{d}\Omega} &= \frac{c\varepsilon_0}{\pi} \sum_{j=1}^{N_p} \int_0^{+\infty} |\mathfrak{F}[\mathbf{u}_j(t)](\omega)|^2 \, \mathrm{d}\omega \\ &= \int_0^{+\infty} \frac{c\varepsilon_0}{\pi} \sum_{j=1}^{N_p} |\mathfrak{F}[\mathbf{u}_j(t)](\omega)|^2 \, \mathrm{d}\omega. \end{aligned} \quad (16)$$

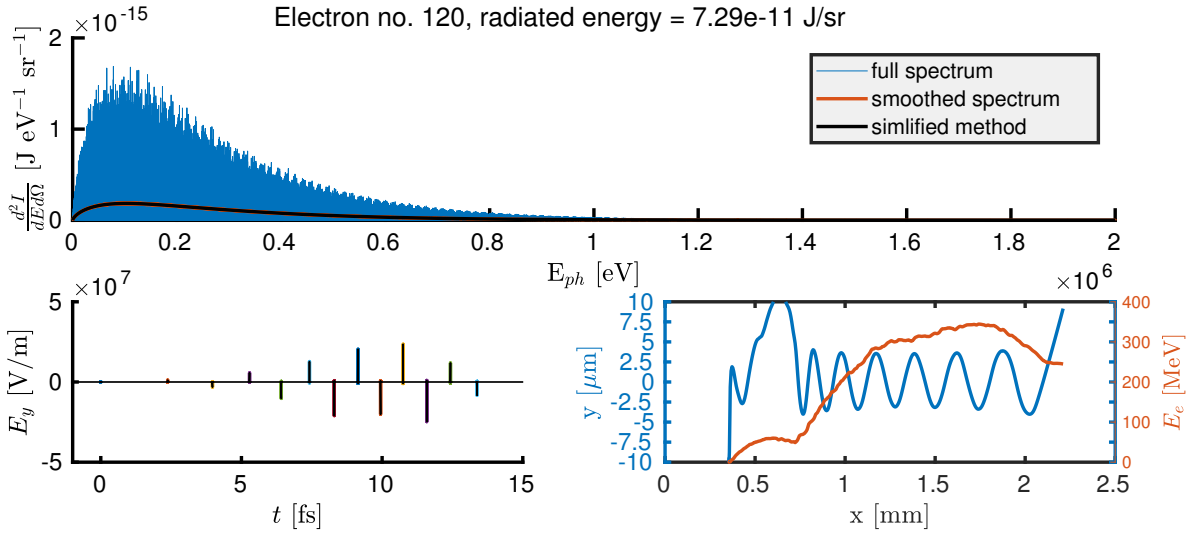

FIG. 4. Upper row: Radiated spectrum by a moving electron on axis for the electron trajectory taken from simulation introduced in Section III A Blue: calculated using general approach. Brown: blue line smoothed using moving average window technique. Black: corresponding spectrum calculated as a sum of contributions by single peaks. Bottom left: Radiation signal $E_y(t)R(t)$ (black) and chosen separated peaks. Bottom right: Electron trajectory in xy-plane (blue, left axis) and evolution of electron energy (brown, right axis).

Hence the spectral intensity of the radiation is similar as in the equation (6)

$$\frac{\mathrm{d}^2 I}{\mathrm{d}\omega \mathrm{d}\Omega} = \frac{c\varepsilon_0}{\pi} \sum_{j=1}^{N_p} \left| \mathfrak{F}[\mathbf{u}_j(t)](\omega) \right|^2 . \tag{17}$$

In conclusion, the calculation of the radiation emitted by single electron in the wiggler case can be simplified to the calculation of the sum of the contributions to the radiation emitted in N_p turning points of its sine-like trajectory

$$\frac{\mathrm{d}^2 I}{\mathrm{d}\omega \mathrm{d}\Omega} = \sum_{j=1}^{N_p} \left. \frac{\mathrm{d}^2 I}{\mathrm{d}\omega \mathrm{d}\Omega} \right|_j . \tag{18}$$

Therefore the long time interval can be replaced by several much shorter ones, which is particularly helpful when high energy radiation is expected and the length of the signal due to huge sampling rate places high demands on the memory.

The radiation spectrum of the 150 MeV electron oscillating with the betatron amplitude 1.2 μm (wiggler case from the Figure 2) calculated as a sum of contributions to the radiation by single peaks is practically equal to its smoothed spectrum calculated according to the equation (6) as can be seen in Figure 3b.

Additionally, similar demonstration was performed also for more realistic problem, namely for the example electron trajectory from PIC simulation. This trajectory was taken from simulation, which will be introduced in Section III A. Figure 4 claims that the radiation spectrum calculated using simplified method is practically indistinguishable from the one obtained by general approach, if this is smoothed. The information about fine structure is lost using the smoothing or the simplified method though.

If the incoherence nature of the electrons in the bunch is assumed, the radiation power emitted by an electron bunch is equal to the sum of powers emitted by each electron[1]. Adapting the simplification introduced above, the total radiation emitted by a bunch containing N_e electrons can be written as

$$\frac{\mathrm{d}^2 I}{\mathrm{d}\omega \mathrm{d}\Omega} = \sum_{i=1}^{N_e} \sum_{j=1}^{N_{p,i}} \left. \frac{\mathrm{d}^2 I}{\mathrm{d}\omega \mathrm{d}\Omega} \right|_{ij} = \sum_{k=1}^{N_P} \left. \frac{\mathrm{d}^2 I}{\mathrm{d}\omega \mathrm{d}\Omega} \right|_k , \tag{19}$$

because all the contributions to the total radiation by all electrons are summed up and it does not depend on the order of the summation.

As the trajectories of individual electrons in the beam differ, the spectra of emitted radiation do not show the same fine structure. Therefore, the fine structure in Figure 4 is likely the feature only of the radiation by single particle, and it vanishes when summing the spectra of N_e particles.

D. Spectrogram: temporal evolution of radiation profile

We can define the quantity of radiated energy per unit frequency and per unit solid angle received during certain time interval $t \in [\tau - \Delta\tau, \tau + \Delta\tau]$ as

$$\left. \frac{\mathrm{d}^2 I}{\mathrm{d}\omega \mathrm{d}\Omega} \right|_{t\in[\tau-\Delta\tau,\tau+\Delta\tau]} = \sum_{k|t_k\in[\tau-\Delta\tau,\tau+\Delta\tau]} \left. \frac{\mathrm{d}^2 I}{\mathrm{d}\omega \mathrm{d}\Omega} \right|_k . \tag{20}$$

In a practical implementation, every time moment t_k when the peak of the radiation by any single electron occurs is stored and total radiation received during time interval $t \in [t_{k_i}, t_{k_{i+1}}]$ is summed up applying the equation (20). In further text, the quantity $\left.\frac{\mathrm{d}^2 I}{\mathrm{d}\omega \mathrm{d}\Omega}\right|_{t\in[\tau-\Delta\tau,\tau+\Delta\tau]}$ will be marked as $\frac{\mathrm{d}^3 I}{\mathrm{d}t\mathrm{d}\omega\mathrm{d}\Omega}$ (or rather $\frac{\mathrm{d}^3 I}{\mathrm{d}t\mathrm{d}E\mathrm{d}\Omega}$, since energy spectrograms will be plotted).

III. ULTRASHORT BETATRON X-RAY PULSES

Three different configurations of LWFA are considered and corresponding radiation spectra are calculated applying the method introduced in previous section. The time profiles of betatron radiation from three different configurations of laser wakefield acceleration setup are determined as well. First one is standard configuration of bubble regime available with 100 TW class laser systems[4]. Second case investigates the scheme of optical injection by transverse laser pulse under similar conditions[27]. It enables significant shortening of the X-ray pulse duration to values below 3 fs. Third one is the experimental configuration using sub-10 TW laser system employing ionization injection[28]. The EPOCH 2D code[29] extended by particle tracker subroutine was used to perform PIC simulations of laser wakefield electron acceleration and to store the trajectories of trapped particles.

Simulation properties were following: simulation box size was 120 μm×60 μm (moving window), grid resolution was 30 cells per wavelength in longitudinal direction and 6 cells per wavelength in transverse direction. There were 3 electron macroparticles per cell in examples presented in Sections III A and III B. In Section III C, one oxygen and one nitrogen macroparticle were placed in every cell at the beginning of simulation, and macroparticles represinting electrons were initialized during the simulation.

A. Radiation features of plasma betatron driven by 100 TW laser

The 40 fs, 800 nm Gaussian laser pulse with laser strength parameter $a_0 = eA_{max}/m_e c^2 = 4$, where A_{max} is maximum value of vector potential, and m_e is the electron rest mass, interacts with transversally homogeneous 2 mm thick plasma layer with electron density $n_e = 1.5\times10^{19}$ cm^{-3} and 40 μm long linear density ramps on both sides in the propagation direction. The focus is located at the end of the front ramp and the waist size (radius at 1/e^2 of maximum intensity) is 9 μm.

The PIC simulation has shown, that electrons self-injection into the ion cavity is continuous. Electron energy spectrum is therefore continuous as well, with maximum energy around 380 MeV. The spectrogram of the radiation calculated using the stored trajectories of 5 000 randomly selected trapped macroparticles (≈ 24% of all of them)[3] is depicted together with its time and energy integrals in Figure 5. Critical energy of the radiation is 127 keV, X-ray pulse length is 13.7 fs (FWHM). Although there are additional X-ray pulses occurring 40 fs before and 70 fs after the main pulse, their intensities are much weaker.

Generated pre-pulse and post-pulse can be conveniently removed using suitable transmission filter. The impact of the usage of 2 mm thick lead filter on generated X-rays is represented on spectrogram in Figure 5b. The values of X-ray mass attenuation coefficients were taken from[30]. Figure 5c illustrates the change of the radiation energy spectrum after propagation through above mentioned filter. Relatively low energy radiation is fully absorbed, whereas the high energy tail remains uninfluenced. Figure 5d shows temporal profile of radiated power and confirms the elimination of pre- and post-pulses.

B. Short X-ray pulses from optical injection configuration by crossed beams with transverse polarizations

The 20 years old Umstadter proposal of optical injection mechanism[31] is recovered and applied on the conditions available with current 100 TW laser systems. A standard configuration of the bubble regime with $a_0 = 4$, $w_0 = 9$ μm, $\tau = 24.9$ fs, $n_e = 4\times10^{18}$ cm^{-3} is used. Lower value of electron density was chosen to avoid self-injection. Injection pulse comes from the orthogonal direction, waist size and the duration are the same as these of the plasma wave driving pulse, but the pulse energy is 100× lower, i.e. the laser strength parameter is $a_0' = 0.4$. Polarization vectors are in the same plane, foci are in the same spot and pulses arrives at the same time[27]. The plasma layer is 2 mm thick, similarly as in Section III A. 10 000 trapped macroparticles (≈ 55% of all of them) were used to calculate the spectrogram of radiation.

Short electron bunch injected into the bubble is depicted in Figure 6a. The electron spectrum is quasi-monoenergetic with peak energy of 530 MeV and relative energy spread of 8 % when the bunch is leaving the plasma layer. Thanks to the short length of the electron bunch ($L = 1.95$ μm), the estimated duration of the X-ray pulse is short as well. The X-ray pulse length is 2.64 fs (FWHM), its critical energy is 54.3 keV.

[3] The sample of trapped macroparticles must well represent the properties of injected electron bunch. Based on authors' experience, at least 5% of trapped macroparticles should be tracked to provide sufficiently accurate result.

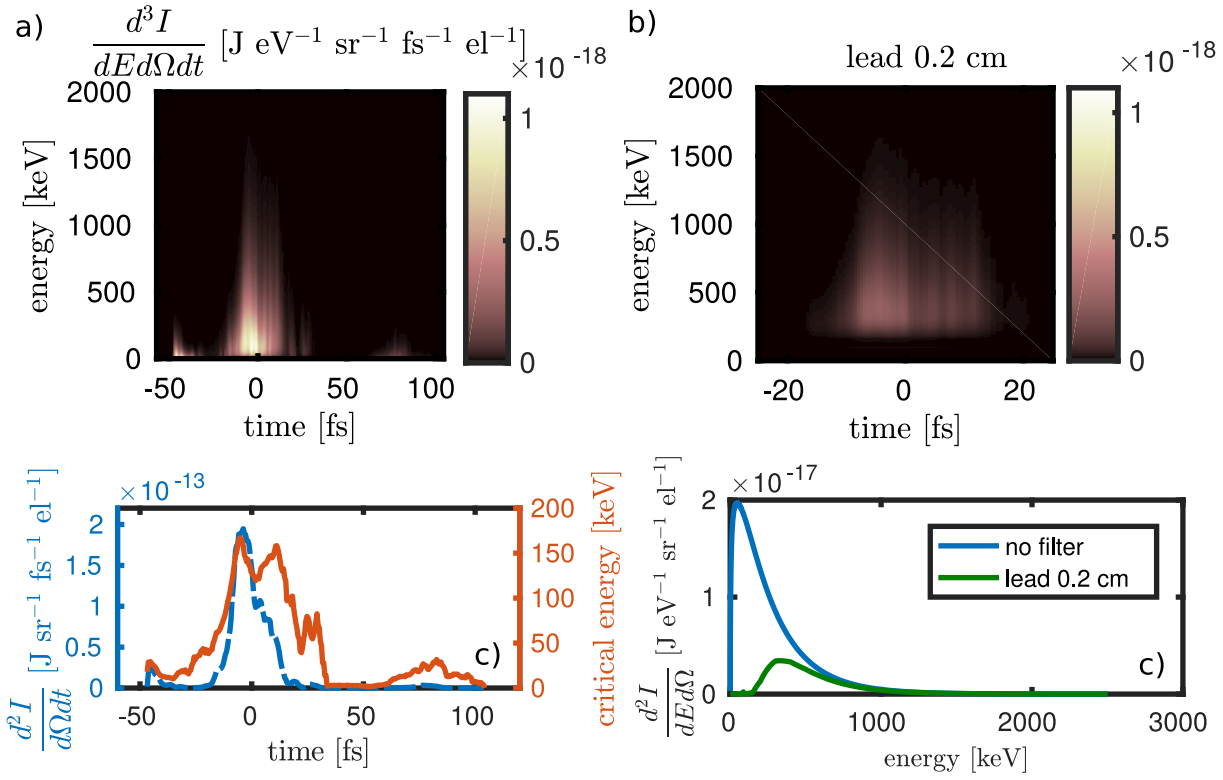

FIG. 5. Betatron radiation from standard LWFA experiment ($\tau = 40$ fs, $\lambda = 800$ nm, $a_0 = 4$, $w_0 = 9$ μm, $n_e = 1.5{\times}10^{19}$ cm^{-3}). a) Original spectrogram without any filter. b) Radiation spectrogram filtered using 2 mm lead foil. c) Total energy spectrum on axis without (blue) and with 2 mm lead filter (green). d) Temporal profile of radiated power (left axis) on axis without (blue solid) and with filter (green dot dashed). Temporal evolution of critical energy (red dotted, right axis).

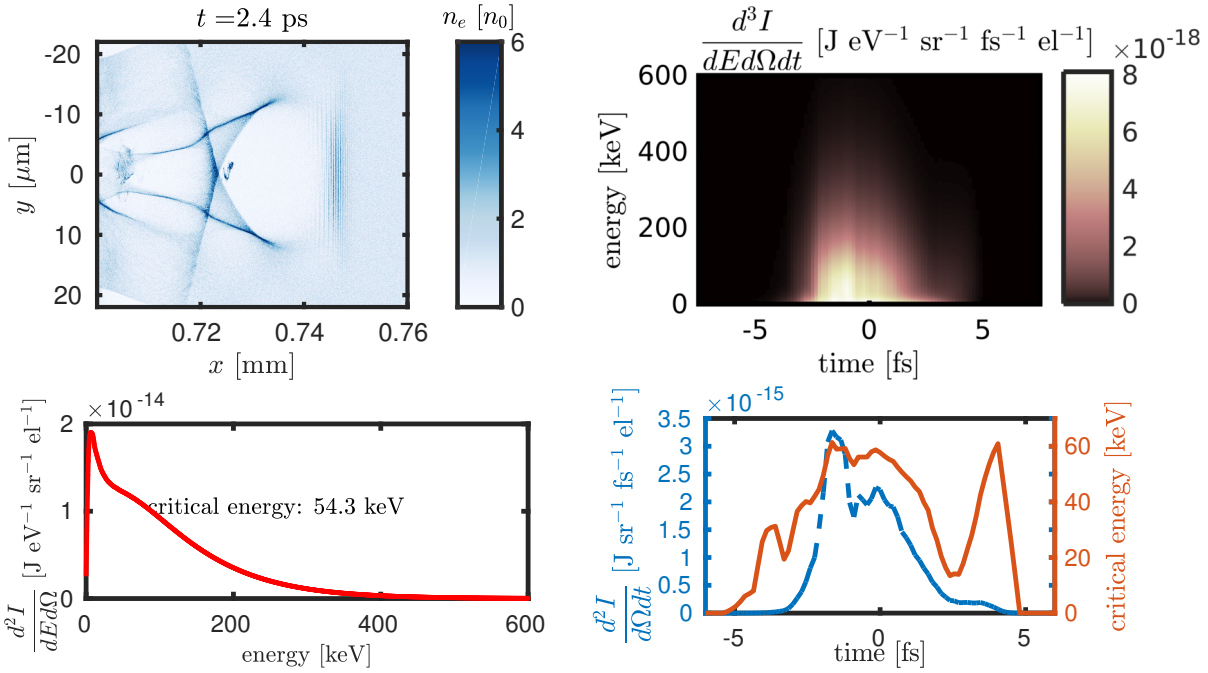

FIG. 6. Betatron radiation in the case of optical injection. a) Electron number density. The bubble with short electron bunch is apparent. b) X-ray spectrogram. c) Total energy spectrum on axis, critical energy is 54.3 keV. d) Temporal profile of radiated power on axis (blue dashed, left axis), pulse duration is 2.64 fs (FWHM), and temporal evolution of critical energy (brown solid, right axis).

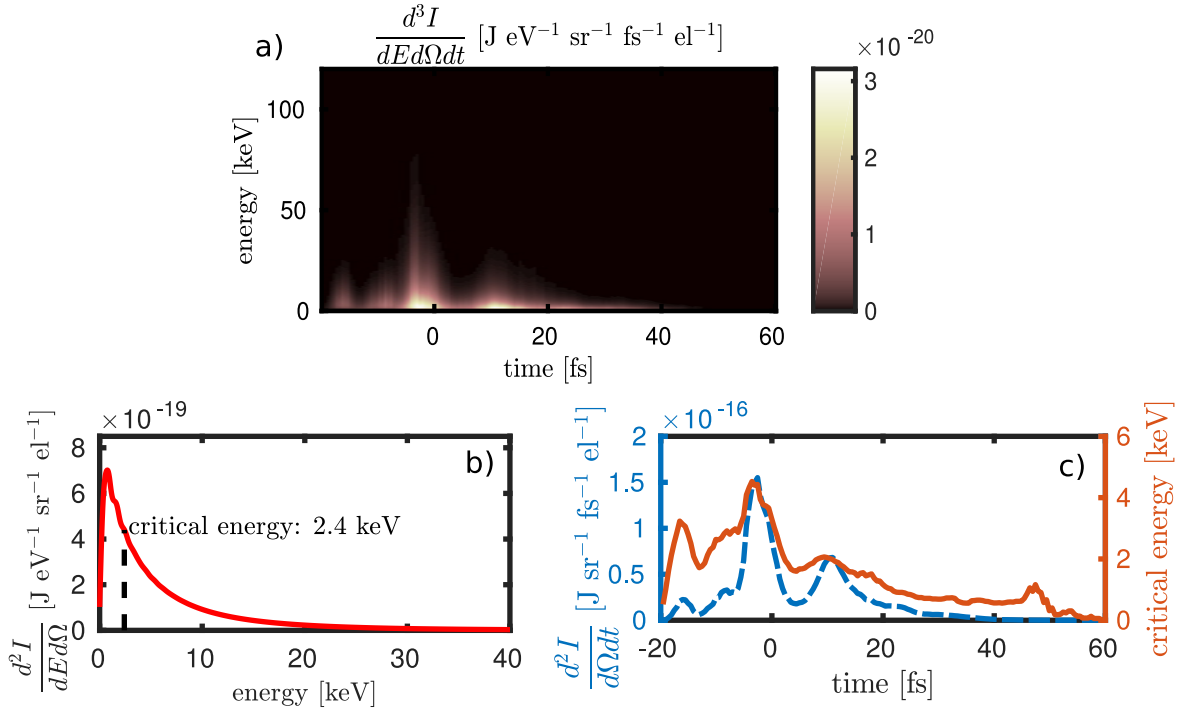

FIG. 7. Radiation calculated using data obtained from the numerical PIC simulation with the input parameters of the experiment run at PALS. a) Spectrogram. b) Total energy spectrum on axis with critical energy 2.4 keV. c) Temporal profile of on axis radiated power (blue dashed line, left axis), pulse duration is approximately 30 fs, and temporal evolution of critical energy (brown solid line, right axis).

Comparisons between both configurations

Despite the similar characteristics of the laser pulse in Sections III A and III B, the betatron radiation characteristics differs significantly. The higher electron density and also higher amplitude of betatron oscillations in Section III A leads to higher critical energy of betatron radiation. On the other hand, Section III B suggests the generation of shorter X-ray pulse. The duration of X-ray pulse depends mainly on the length of the injected electron bunch L. However, it is worth noting that our calculation suggests that this duration is shorter than classical estimate L/c, which would be 6.5 fs for the case introduced in Section III B.

Total number of radiated photons at mean photon energy (i.e. ≈ 0.3 of critical energy) per trapped electron is 0.95 for self-injection case, 0.54 for optical injection case. The higher injected charge in the self-injection scheme ($\approx 10\times$, estimate from 2D simulation) leads to higher ($\approx 17.5\times$) intensity of betatron radiation in this case.

C. Sub-10 TW laser driven electron accelerator with ionization injection: Experiment and simulation

Experimental campaign focused on laser wakefield electron acceleration was carried out with Ti:sapphire laser system at PALS facility in Prague in 2016[32]. The setup was following: 50 fs, 0.36 J, 810 nm laser pulse interacted with the supersonic dry air target. The electron density measured by Mach-Zehnder interferometer was around 5×10^{19} cm^{-3}. The laser beam was focused to the spot with the size 14 μm horizontally and 10 μm vertically.

Highly stable electron bunches with mean energy 17 MeV and energy spread 14 MeV (root mean squared) were measured. Corresponding PIC simulations of the interaction of above described laser pulse with the neutral gas target were carried out to support this observation. Field ionization according to the ADK model[33], barrier suppression ionization, and multiphoton ionization are included in the EPOCH code[34]. The initial atomic densities of gases were $n_O = 1.15 \times 10^{18}$ cm^{-3} and $n_N = 8.02 \times 10^{18}$ cm^{-3} for oxygen and nitrogen, respectively.

The peak electron energy of 17.1 MeV with energy spread of 12.1 MeV obtained from the simulations was confronted with the measured data (see Fig. 8). Good agreement between these spectra was confirmed. The simulated spectrum shown in the figure comes from the time 1.7 ps after the moment when the laser pulse reached the focal spot. Numerical PIC simulation indicates that due to high plasma density the phase velocity of the plasma wave is low and therefore the electrons are not accelerated to higher energies, not even in later times.

The trajectories of the representative sample of the trapped electrons were tracked (3 000 macroparticles i.e.

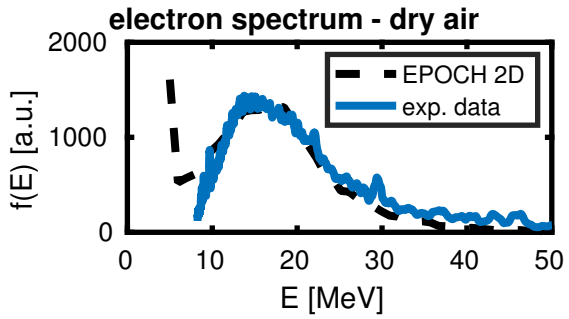

FIG. 8. Electron spectra (blue solid) measured and simulated (black dashed).

≈ 15% of all of them). The spectrogram of the radiation calculated using our method is presented in Figure 7. The shape of the X-ray spectrogram is well reflecting the fact that there were two moments of injection in the simulation. The length of the X-ray signal is approximately 30 fs and the critical energy is 2.4 keV.

IV. CONCLUSION

We have investigated the temporal profile of the betatron radiation generated using the conditions of a typical bubble LWFA regime, and a configuration with ionization injection used during the experimental campaign at PALS laboratory. The calculations presented indicate that generated X-ray pulse durations are typically shorter then driver laser pulse duration. Furthermore, a mechanism to generate X-ray pulses shorter than 3 fs is proposed.

The properties of betatron radiation are calculated from the trajectories of the accelerated electrons using a newly developed method. In this method, the X-ray spectrum is calculated using the Fourier transform of the electric field emitted by relativistic electrons. The core of the method is based on the fact that the electron oscillating in the wiggler regime emits radiation almost exclusively in the turning points of its sine-like trajectory. Therefore only few very narrow time intervals contribute significantly to betatron radiation emission and the rest of the signal is neglected, which makes the calculation computationally efficient compared to traditional methods. The method is exploitable for standard betatron radiation energies ($E_{ph} < 10$ MeV), since quantum effects are not taken into account.

The knowledge of time moments of radiation peaks by any single electron enables us to construct the spectrogram of the radiation using our method, if the incoherent nature of the electron bunch is assumed. Hence, the method offers the estimation of the temporal profile of betatron radiation, i.e. the characteristic which can be measured only using sophisticated pump-probe techniques that, to our knowledge, have not been performed experimentally.

We believe that our method represents useful tool to investigate or to tailor the betatron X-ray pulse temporal profiles and it can be used to design sources for future applications such as probing of ultrafast fundamental physical processes.

ACKNOWLEDGMENTS

Authors wish to acknowledge financial support from Czech Science Foundation (GA ČR) project 15-03118S, Czech Technical University (CTU) project SGS16/248/-OHK4/3T/14, ELI - Extreme Light Infrastructure - phase 2 (CZ.02.1.01/0.0/0.0/15_008/0000162) and Creating and probing dense plasmas at the PALS facility (CZ.02.1.010.00.016_0130001552) projects from European Regional Development Fund, and Project LQ1606 of the Ministry of Education, Youth and Sports of the Czech Republic as part of targeted support from the National Programme of Sustainability II. The financial support provided by the Ministry of Education, Youth and Sports of the Czech Republic within the projects LM2015042 (CESNET), LM2015083 (PALS), and LD14089 is greatly appreciated.

[1] S. Corde, K. T. Phuoc, G. Lambert, R. Fitour, V. Malka, A. Rousse, A. Beck, and E. Lefebvre, "Femtosecond X-rays from laser-plasma accelerators," Reviews of Modern Physics **85**, 1 (2013).

[2] A. Rousse, K. T. Phuoc, R. Shah, A. Pukhov, E. Lefebvre, V. Malka, S. Kiselev, F. Burgy, J.-P. Rousseau, D. Umstadter, *et al.*, "Production of a keV X-ray beam from synchrotron radiation in relativistic laser-plasma interaction," Physical Review Letters **93**, 135005 (2004).

[3] S. Kiselev, A. Pukhov, and I. Kostyukov, "X-ray Generation in Strongly Nonlinear Plasma Waves," Physical Review Letters **93**, 135004 (2004).

[4] E. Esarey, C. Schroeder, and W. Leemans, "Physics of laser-driven plasma-based electron accelerators," Reviews of Modern Physics **81**, 1229 (2009).

[5] T. Tajima and J. Dawson, "Laser electron accelerator," Physical Review Letters **43**, 267 (1979).

[6] K. Yamanouchi, S. Cundiff, R. de Vivie-Riedle, M. Kuwata-Gonokami, and L. DiMauro, *Ultrafast Phenomena XIX: Proceedings of the 19th International Conference, Okinawa Convention Center, Okinawa, Japan, July 7-11, 2014*, Vol. 162 (Springer, 2015).

[7] R. D. Miller, "Femtosecond crystallography with ultrabright electrons and X-rays: capturing chemistry in action," Science **343**, 1108–1116 (2014).

[8] N. Bloembergen, "From nanosecond to femtosecond science," Reviews of Modern Physics **71**, S283 (1999).

[9] A. Rousse, C. Rischel, and J.-C. Gauthier, "Femtosecond X-ray crystallography," Reviews of Modern Physics **73**, 17 (2001).

[10] H. N. Chapman, P. Fromme, A. Barty, T. A. White, R. A. Kirian, A. Aquila, M. S. Hunter, J. Schulz, D. P. DePonte, U. Weierstall, *et al.*, "Femtosecond X-ray protein nanocrystallography," Nature **470**, 73–77 (2011).

[11] V. Levitin, *Atom Vibrations in Solids: Amplitudes and Frequencies*, Physics Reviews Series (Cambridge Scientific Publishers Limited, 2004).

[12] A. Thomas, "Algorithm for calculating spectral intensity due to charged particles in arbitrary motion," Physical Review Special Topics-Accelerators and Beams **13**, 020702 (2010).

[13] M. Chen, E. Esarey, C. G. R. Geddes, C. B. Schroeder, G. R. Plateau, S. S. Bulanov, S. Rykovanov, and W. P. Leemans,

"Modeling classical and quantum radiation from laser-plasma accelerators," Physical Review Special Topics - Accelerators and Beams **16** (2013).
[14] J. D. Jackson, *Classical electrodynamics* (Wiley, 1999).
[15] A. J. Jerri, "The Shannon sampling theorem—Its various extensions and applications: A tutorial review," Proceedings of the IEEE **65**, 1565–1596 (1977).
[16] F. Tsung, W. Lu, M. Tzoufras, W. Mori, C. Joshi, J. Vieira, L. Silva, and R. Fonseca, "Simulation of monoenergetic electron generation via laser wakefield accelerators for 5–25 TW lasers," Physics of Plasmas **13**, 056708 (2006).
[17] J. A. Fessler and B. P. Sutton, "Nonuniform fast Fourier transforms using min-max interpolation," Signal Processing, IEEE Transactions on **51**, 560–574 (2003).
[18] J. F. Kenney and E. S. Keeping, *Mathematics of statistics* (JSTOR, 1965).
[19] E. Esarey, B. Shadwick, P. Catravas, and W. Leemans, "Synchrotron radiation from electron beams in plasma-focusing channels," Physical Review E **65**, 056505 (2002).
[20] J. Ju, *Electron acceleration and betatron radiation driven by laser wakefield inside dielectric capillary tubes*, Ph.D. thesis, Universite Paris-Sud XI (2013).
[21] A. Rousse, K. T. Phuoc, R. Shah, A. Pukhov, E. Lefebvre, V. Malka, S. Kiselev, F. Burgy, J.-P. Rousseau, D. Umstadter, and D. Hulin, "Production of a keV X-Ray beam from synchrotron radiation in relativistic laser-plasma interaction," Physical Review Letters **93**, 135005 (2004).
[22] K. T. Phuoc, S. Corde, R. Shah, F. Albert, R. Fitour, J.-P. Rousseau, F. Burgy, B. Mercier, and A. Rousse, "Imaging electron trajectories in a laser-wakefield cavity using betatron X-ray radiation," Physical Review Letters **97**, 225002 (2006).
[23] S. Kneip, S. Nagel, C. Bellei, N. Bourgeois, A. Dangor, A. Gopal, R. Heathcote, S. Mangles, J. Marques, A. Maksimchuk, *et al.*, "Observation of synchrotron radiation from electrons accelerated in a petawatt-laser-generated plasma cavity," Physical Review Letters **100**, 105006 (2008).
[24] S. Mangles, G. Genoud, S. Kneip, M. Burza, K. Cassou, B. Cros, N. Dover, C. Kamperidis, Z. Najmudin, A. Persson, *et al.*, "Controlling the spectrum of X-rays generated in a laser-plasma accelerator by tailoring the laser wavefront," Applied Physics Letters **95**, 181106 (2009).
[25] S. Fourmaux, S. Corde, K. T. Phuoc, P. Leguay, S. Payeur, P. Lassonde, S. Gnedyuk, G. Lebrun, C. Fourment, V. Malka, *et al.*, "Demonstration of the synchrotron-type spectrum of laser-produced betatron radiation," New Journal of Physics **13**, 033017 (2011).
[26] A. A. Andreev, A. L. Galkin, M. P. Kalashnikov, V. V. Korobkin, M. Y. Romanovsky, and O. B. Shiryaev, "Electrons in a relativistic-intensity laser field: generation of zeptosecond electromagnetic pulses and energy spectrum of the accelerated electrons," Quantum Electronics **41**, 729–734 (2011).
[27] V. Horný, V. Petržílka, M. Krůs, and O. Klimo, "Electron acceleration in perpendicularly crossed laser beams with following injection in the laser wakefield accelerator," in *Proceedings of the 43rd EPS Conference on Plasma Physics* (2016).
[28] C. Clayton, J. Ralph, F. Albert, R. Fonseca, S. Glenzer, C. Joshi, W. Lu, K. Marsh, S. Martins, W. Mori, *et al.*, "Self-guided laser wakefield acceleration beyond 1 GeV using ionization-induced injection," Physical Review Letters **105**, 105003 (2010).
[29] "EPOCH:Extendable PIC Open Collaboration," `https://ccpforge.cse.rl.ac.uk/gf/project/epoch/` (2016), accessed: 2016-12-20.
[30] J. H. Hubbell and S. M. Seltzer, "Tables of X-ray mass attenuation coefficients and mass energy-absorption coefficients 1 keV to 20 MeV for elements Z= 1 to 92 and 48 additional substances of dosimetric interest," Tech. Rep. (National Inst. of Standards and Technology-PL, Gaithersburg, MD (United States). Ionizing Radiation Div., 1995).
[31] D. Umstadter, J. Kim, and E. Dodd, "Laser injection of ultrashort electron pulses into wakefield plasma waves," Physical Review Letters **76**, 2073 (1996).
[32] K. Boháček, M. Kozlová, J. Nejdl, U. Chaulagain, V. Horný, M. Krůs, and M. Albrecht, "Generation of laser-driven femtosecond electron beams for secondary photon sources with 7 TW Ti-sapphire laser system at PALS," in *Proceedings of the 43rd EPS Conference on Plasma Physics* (2016).
[33] M. Ammosov, N. Delone, V. Krainov, A. Perelomov, V. Popov, M. Terent'ev, G. L. Yudin, and M. Y. Ivanov, "Tunnel ionization of complex atoms and of atomic ions in an alternating electric field," Sov. Phys.—JETP **64**, 1191–1194 (1986).
[34] T. Arber, K. Bennett, C. Brady, A. Lawrence-Douglas, M. Ramsay, N. Sircombe, P. Gillies, R. Evans, H. Schmitz, A. Bell, *et al.*, "Contemporary particle-in-cell approach to laser-plasma modelling," Plasma Physics and Controlled Fusion **57**, 113001 (2015).